Optical Materials 73 (2017) 25–32

Contents lists available at ScienceDirect

Optical Materials

journal homepage: www.elsevier.com/locate/optmat

Optical waveguides fabricated in Cr:LiSAF by femtosecond laser micromachining

Demian A. Biasetti [a, b, c], Emiliano J. Di Liscia [d], Gustavo A. Torchia [a, b, e, *]

[a] Centro de Investigaciones Ópticas, Argentina
[b] CONICET La Plata, CICBA, Argentina
[c] Universidad Nacional de La Plata, Argentina
[d] Comisión Nacional de Energía Atómica, Argentina
[e] Departamento de Ciencia y Tecnología, Universidad Nacional de Quilmes, Argentina

ARTICLE INFO

Article history:
Received 9 May 2017
Received in revised form
4 July 2017
Accepted 19 July 2017

Keywords:
Ultrafast laser inscription
Waveguides characterization
Micro-luminescence
Cr:LiSAF

ABSTRACT

In this work we present the fabrication of double-track type II waveguides written in 1% doped Cr:LiSrAlF$_6$ (Cr:LiSAF) crystal by femtosecond laser micromachining. We studied waveguides fabricated at energies from 1 to 7 μJ per pulse at writing speeds of 15–45 μm/s. We found good wave-guiding performance for both, Transversal Magnetic (TM) and Transversal Electric (TE) polarization modes as well as acceptable losses according to the expected values addressed to technological applications. Also, we performed a high-resolution μ-luminescence waveguide cross-section mapping between the tracks, in order to identify possible spectral changes caused for active ions Cr^{3+} corresponding to the $^4T_2 \rightarrow {}^4A_2$ vibronic transition in the focal volume zone, due to induced anisotropic graded stress. Finally, their lifetimes were measured for bulk as well as for waveguide trapped ions. We found that for the range of parameters of ultra-short micromachining used, the Cr^{3+} ions embedded in the waveguides remained spectroscopically unchanged compared with those observed in bulk material.

1. Introduction

In the last decades, one of the main goals of photonic researchers has been the development of low-cost, compact, and robust ultrafast lasers suitable for a wide range of applications such as medicine, microscopy, and imaging, among others. Portability and low noise of these devices become especially useful for diagnostic measurements out of the laboratory. The current investigations in the fabrication technologies for waveguides in optical crystals are devoted to achieving new lasers with the mentioned properties. In this way, optical waveguides femtosecond micromachining has become a worldwide fabrication method due to the reduction of the number of fabrication stages, the possibility of three-dimensional designs, and also the wide range of materials suitable for processing by this method [1,2].

By choosing an adequate lens, a tight focal volume zone of the femtosecond laser pulses can be achieved by applying the femtosecond writing technique in different materials. Thus, it is possible to induce controlled changes in the refractive index so that low cross-sections in the resultant waveguides can be reached [2–4]. For the so called Type II waveguides [2], the guiding cross-section depends on the extension of the optical breakdown filament generated as well as on the separation between tracks and wavelength to be propagated.

On the other hand, luminescence and spectroscopic properties of doped materials play an important role in the fabrication of optical devices, display technologies and the laser industry. The femtosecond writing technique in both new and well-known active optical materials is an interesting tool because it can offer new technological potential for the fabrication of many photonic integrated systems, in particular integrated laser devices.

Rare earths (RE) and transition metals ions (TMI) are well-known candidates to perform these applications [5–7]. Nowadays, tunable all-solid-state lasers have become useful for many applications in different fields. For instance, Cr ions are one of the most used and appropriate active dopant in different hosts, as reported in the literature [7]. In particular, good spectroscopic and lasing properties of Cr:LiSAF are well known [7–11]. As examples of spectroscopic ones, we can mention a broader lasing range (780–1060 nm), a considerable stimulated emission cross-section

* Corresponding author. Centro de Investigaciones Ópticas, Argentina.
E-mail address: gustavot@ciop.unlp.edu.ar (G.A. Torchia).

http://dx.doi.org/10.1016/j.optmat.2017.07.042
0925-3467/

of 4.8 × 10^{-20}cm^2 (electric field ||c, at 846 nm of peak emission wavelength), and a sufficiently large lifetime of $^4T_2 \rightarrow {}^4A_2$ transition. The last mentioned characteristic implies a low laser power threshold.

Pumping can be carried out by using flash-lamp or laser diodes of GaInP/AlGaInP peaking at 670 nm [12,13]. In fact, different laser configurations [12–18] of femtosecond tunable lasers have been reported and discussed with that crystal, especially for mode-locked setups.

From a phenomenological point of view, TMI in bulk material could work as a direct tester of morphological changes, and it has also been demonstrated that micro-luminescence spectroscopy provides useful information about stress in written waveguides made in RE doped crystals, particularly in Nd:YAG [19]. In this sense must be mentioned that the TMI with non-zero spin configuration have high spectroscopic sensitivity to environmental changes. This fact can be predicted from the Tanabe-Sugano (TS) diagram [20,21], which shows the vibronic transition when the field strength around active ions is increased or decreased. For instance, the induced stress after laser writing could affect the luminescence transitions because the shifting in the peak of the luminescence transition depends, according to the TS model, on the energy level slopes in these diagrams, in which, essentially, the energy versus strength field is plotted. In different real crystals, although a numerical calculus of field strength as a function of strain can be made, taking into account the primitive cell geometry, the way that strain is induced by femtosecond laser interaction in each particular cell is still unpredictable. Therefore, quantitative results about spectroscopic transitions for ions depend on morphological changes induced by ultrafast laser inscription (ULI) so by this analysis it is expectable to retrieve evidence about the intensity of the induced stress after laser processing.

Another typical parameter studied in active ion-doped crystals considered for laser applications is the luminescence lifetime from laser transition levels. This parameter can be an adequate probe for fluctuations such as degree of doping or working temperature [21,22]. In the same framework as described above, the lifetime measurements of embedded TMI dopant luminescent transitions could also be considered as evidence of induced crystallographic phase modification by femtosecond processing after nonlinear process carried out in transparent media.

There have been already reported optical waveguides in Cr:LiSAF crystals fabricated by ion implantation technique [23,24] but in this work, for the first time of our knowledge we show suitable optical waveguides in Cr:LiSAF fabricated by ULI. We analyze and discuss their optical performance and spectroscopic features, bearing in mind their potential applications in integrated photonics.

2. Experimental

2.1. Fabrication

Femtosecond laser pulses were produced by a Ti: sapphire Chirped Pulse Amplification (CPA) system from Spectral Physics (Mai-Tai Spitfire). This equipment can deliver a pulse width of 100 fs at a repetition rate of 1 kHz with a center wavelength of around 796 nm. A laser beam using a Leica 20 × objective of 0.4 N.A. was focused 250 μm below the surface of an *a*-cut Cr:LiSAF rectangular sample. Transversal micromachining geometry was used, with transversal polarization of the beam relative to displacement, which in turn was made transversal to *a* and *c* axis. Writing parameters were set at writing speeds of 15, 30 and 45 μm/s and energies per pulse ranging from 1 μJ to 7 μJ. The distances between tracks, which define the waveguide width, were set at 15 and 20 μm for structures written at 1–3 μJ per pulse. The rest of the waveguide widths were 20 μm. Finally, the end edges of the waveguides were polished up to optical grade with diamond powder in order to obtain a high performance light coupling.

2.2. Guiding properties

A standard “end-fire” system [6] was used for measuring the guided modes at the near-field in order to test the guiding performance of the resultant guiding structures. At the input and output, a 20 × microscope objective with an N.A. of 0.4 was used to couple and collect light in the waveguide. The light source used was a He-Ne laser beam with a wavelength of 632.8 nm with a power lower than 30 mW operating at CW. The intensities of the modal profiles were measured by focusing the images onto an 8-bit Newport Beam Profiler analyzer with a charge coupled device detector (CCD). A micro-positioner was used to control the input objective and thus to optimize the coupling of light inside these structures all mode profile images where recorded with the same camera settings under identical experimental conditions.

As the first task, the system was used to evaluate the likelihood of guiding for these structures as a function of the energy per pulse with which they were written. Then, the performance dependence with speed writing and polarization guiding dependence were explored, the latter just by interposing a polarizer between the source and the input objective.

The laser beam was set linearly polarized at 45° being taken the normal to the work table as reference. The polarizer was installed crossing on the pathway between the laser and input waveguides, allowing us to evaluate whether the waveguides can support the *quasi*-TE or *quasi*-TM modes [25].

Otherwise, we have made a complete characterization for the best waveguide fabricated in this work. In this sense, we explore the 20 μm waveguide width written at 3 μJ and 30 μm/s on energy and writing speed, respectively. The insertion losses were estimated by measurements of Fabry-Perot (FP) resonances when a tunable narrow linewidth laser diode at 1550 nm wavelength with a tuning range of 1 nm was launched to the waveguide. Fitting the Airy function of the transmittance of the fundamental mode in the FP resonator, the extinction coefficient was calculated according [26].

2.3. Spectroscopic characterization

Two kinds of spectroscopic characterizations for Cr^{3+} ions were carried out for these guiding structures: on the one hand, μ-luminescence between tracks (inside the waveguide region), and on the other hand, measurements of lifetime of the guided light.

Micro-luminescence spectra from samples were measured using a spectrometer equipped with a confocal microscope (LabRAM HR Raman system, Horiba Jobin Yvon) and a CCD. The 632.8 nm line from a He-Ne laser was the excitation source in the confocal microscope. An 800 g/mm grating and 100 μm hole result in a spectral resolution of 2 cm^{-1} for this system. Every spectrum was collected for both bulk and waveguides. For the latter, a micro-luminescence mapping was performed over the whole waveguide cross-section, with the laser beam (the He-Ne laser source included in the microscope) focused by a 50 × microscope objective at 2 μm below the surface. In this micro-luminescence scan, the measured points were spaced 4 μm apart from each other.

It can be expected, considering the symmetry, that a mapping along the X axis will remain unchanged within the experimental uncertainty. However, given the anisotropy of these structures aside of the optical breakdown zone and because of filamentation effect occur in one direction, changes could be displayed in the

micro-luminescence mapping. Potential spectroscopic variations are more expectable along the Z direction (corresponding with *c*-crystal axis) than in the X direction, bearing in mind that stress decreases moving away from the laser track and also considering a possible accumulative effect of induced stress corresponding to each track along this axis.

On the other hand, in order to pump the $^4T_2$ level and then measure its time decay, insomuch as this level's lifetime is expected to be 67μs for 1% Cr doping (at room temperature, according to the literature [8–11]), a pulsed laser diode with a 0.5μs temporal width, and repetition rate of 2 kHz centered at 650 nm was used. This wavelength is close to the maximum of the absorption peak of Cr:LiSAF crystal. A very short pumping pulse allowed us to avoid the overlap between the luminescence signal and each pulse, thus enabling to measure the whole decay time. The power per pulse was set at around 80 mW, obtaining a good signal-to-noise ratio for the luminescence analysis. Further, the luminescence output signal from the waveguide was focused into a phototube powered by 840 V which in turn was connected to a digital oscilloscope. An adequate resistance was added to set appropriate impedance thus ensuring good gain without losing temporal response. Also, a suitable high pass cut-off optical filter was included in this experiment in order to remove the laser excitation line (crossing on the pathway between output of waveguide and the phototube). For waveguide measurements a pinhole was used to filter the scattering and thus collects only the signal from the modal field.

3. Results and discussion

3.1. Optical guiding performance

First of all, in Fig. 1 we show several optical micrographs of the double-track structure cross-section fabricated in this work for qualitative purposes only. From this figure we can observe that after writing process the filamentation effect in Cr:LiSAF occurs, with our writing setup, for structures made using energies per pulse above 1 μJ in Cr:LiSAF.

In Fig. 2 (a) up to 2 (f), we show the mode intensity profiles for

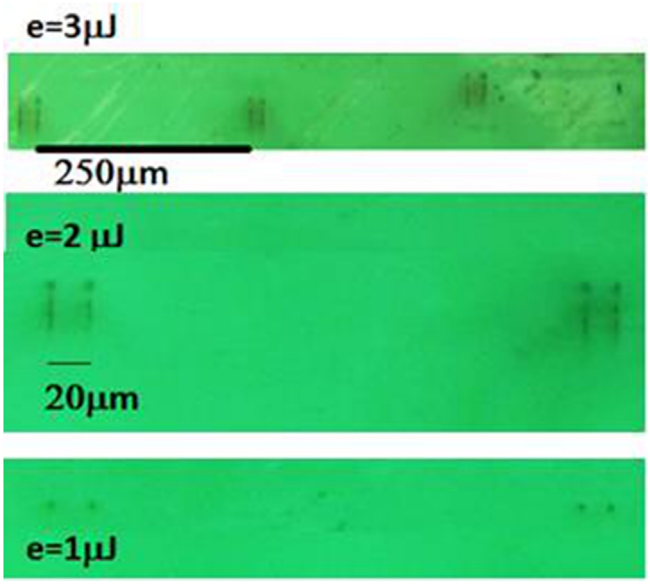

Fig. 1. Optical micrographs taken by reflected light. a) Waveguides written at 3 μJ b) Double-track structures written at 2 μJ per pulse and writing speed of 45 μm/s separated by 20 and 15 μm from left to right. c) The spots (dark points) generated by 1 μJ fs pulses. The micromachining laser beam is coming from the top of the pictures.

double-track structures of 20 μm width obtained following the procedure described in Section 2. These figures show modes corresponding to guiding structures fabricated at 2 μJ (a,b,c) and 3 μJ (d,e,f) per pulse. In these figures three guided modes which correspond to waveguides written at velocities of 15, 30, and 45 μm/s from left to right, are sketched. On the left, a color map scale describes the intensity modal distribution after couple light in identical conditions. As a first result, we can point out that, the writing velocity may not be a relevant fabrication parameter in the range of velocities used in our work being really important the delivered energies on the material. Energy accumulation effect due to overlapping pulses is practically the same in the range of employed velocities, since the overlapping is relatively high (taking into account the focal waist and speed of writing).

On the other hand, the double-track waveguides of 15 μm width made at 2 and 3 μJ per pulse and different writing speeds showed weakly guiding modes for an input wavelength of 632.8 nm. As a consequence of the observed invariance with the velocity for the guiding performance, Fig. 3 shows modes only for waveguides written at 45 μm/s for both energies used. The reduction of optical performance, as can be expected, is related to the reduction in size of the effective waveguide cross-section [24].

For energies above 3 μJ per pulse, we found multimodal waveguides at the same testing wavelength (632.8 nm). Also, due to the greater scattering observed at the border of the guiding mode, we found a more irregular shape of the propagated modes in these new waveguide structures. In order to illustrate this effect, Fig. 5 shows the modes for a double-track structure written at 7 μJ per pulse and writing speed of 30 μm/s. Between the tracks and external side of one of these, the guided light is confined, as it is shown in Fig. 4 (a) and 4(b) respectively. The modal structure shown in (b) is known as a single track waveguide. The multimodal character is expectable considering that filaments were larger because self-focusing effect is reached at higher energies. Also, the possibility of obtaining a guiding mode at the external side of the track was expectable too because higher energies imply a higher induced stress close to the laser track.

Also, it should be highlighted that for double-track structures written at 1 μJ per pulse we found that light guiding is not possible, which may be directly related to the absence of filamentation at this energy. Also we must remark that outside the double-track structure, coupling was not possible for those waveguides written at energies lower than 6 μJ. Fig. 5 show a multimodal double-track waveguide written at 7 μJ per pulse and the light coupling on outside of the laser double-track region.

Concerning to losses measurements, the exponential decay coefficient gives us an upper limit of 1.3 dB/cm with an uncertainty of about 25% attributed to the standard deviation in the results. Although losses at 650 nm and 980 nm of wavelength are expected to be larger due to high Rayleigh scattering dependence, for this kind of waveguides, propagation losses are quite lower than those reported by Ref. [24].

On the other side, one of the most important results reveals that the waveguides can support the two polarizations of the electric field: vertical (quasi-TM mode) and horizontal (quasi-TE mode), as shown in Fig. 5. This figure presents the guided mode for both polarizations corresponding to a double-track waveguide written at 3 μJ. For the other energies, the behavior observed was similar in all cases. The quasi-TM mode was slightly stronger mode than the quasi-TE mode, as can be seen by comparing Fig. 5(b) and (c).

To better understand the polarization behavior of guiding modes we explored all polarization angles of output power after setting equal input power for both field components, corresponding to the x and z axis. In order to do that, we used a He-Ne laser source, linearly polarized at 45° input angle respect to transversal x

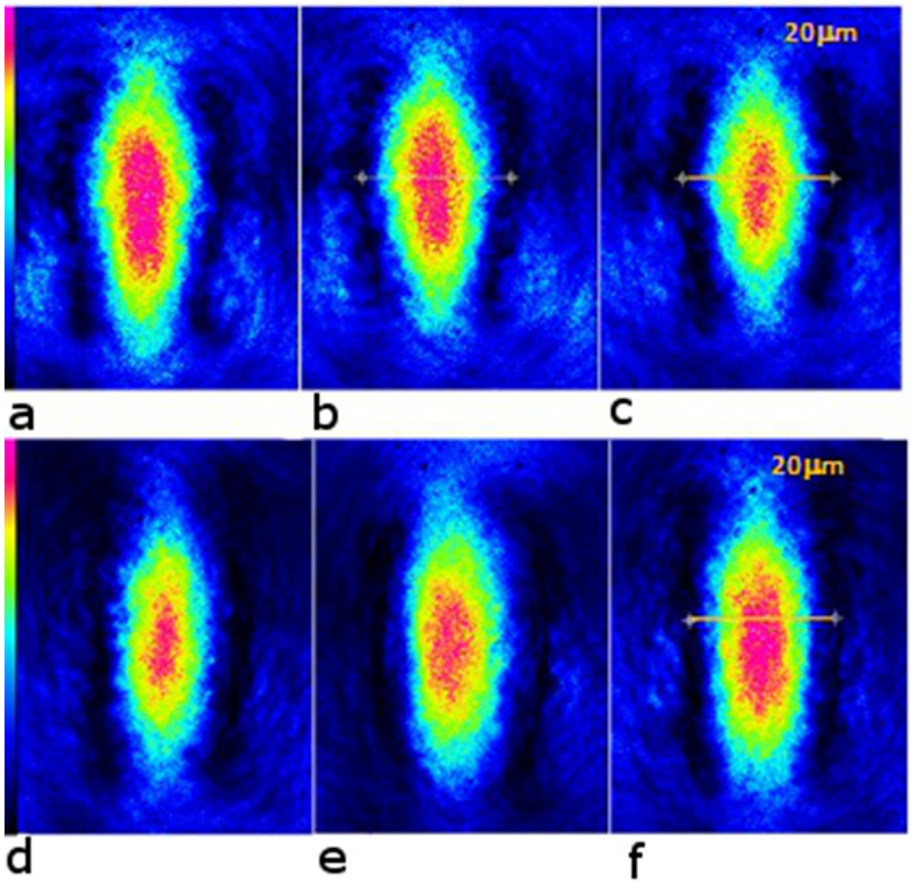

Fig. 2. Modal distribution of double-track waveguides made at (a) 2 and (b) 3 μJ per pulse. The color map scale shown on the left side of pictures illustrates the intensity profiles of modes. The intensity increases from black to red. The writing speeds were: 15, 30, and 45 μm/s from left to right. (For interpretation of the references to colour in this figure legend, the reader is referred to the web version of this article.)

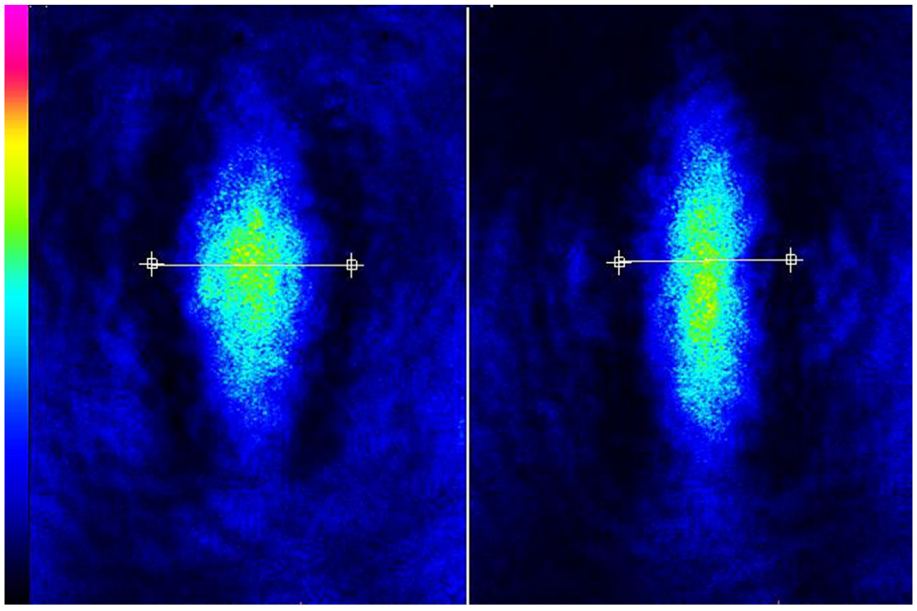

Fig. 3. Modal distribution of double-track waveguides separated by a distance of 15 μm made at 2 and 3 μJ per pulse for (a) and (b) respectively, both written at a writing speed of 45 μm/s.

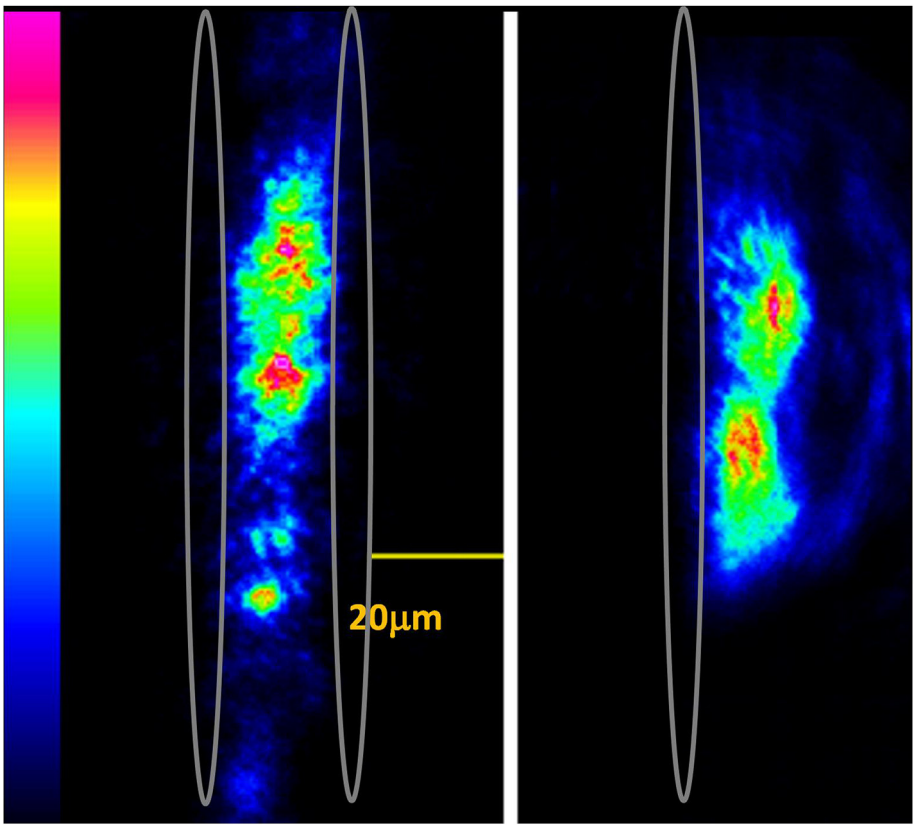

Fig. 4. Modal distribution of double-track waveguides separated a distance of 20 μm made by 7 μJ per pulse, where filaments are represented by grey open ellipses. a) Shows the modal distribution in the core of the double structure and b) shows the mode at the outside of one of the tracks, like a single-track waveguide.

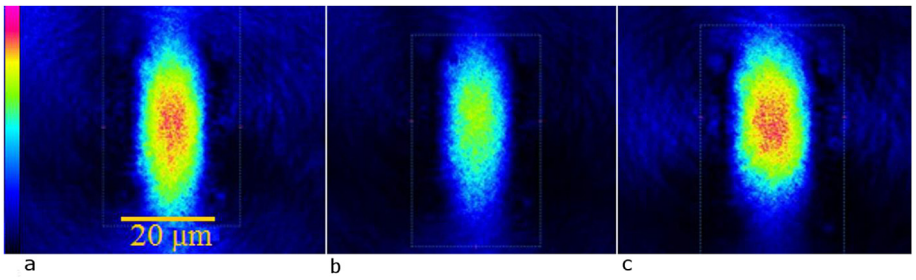

Fig. 5. Double-track waveguide made at 3 mJ and a writing speed of 45 μm/s a) The mode corresponds to that coupling an elliptical polarization input at the waveguide. Then, at the same input power conditions, b and c) correspond to TE and TM modes, respectively. For other waveguides, the guiding polarization behavior was the same.

axis. By using a dichroic crystal after the output microscope objective of the end-fire-system, we imaged onto the CCD camera the corresponding fraction of modal power transmitted. The transmission axis of the output mode system has been gradually rotated between 0 and 360°. In Fig. 6 we show the polar representation of the output field amplitude from both, waveguide and bulk. It becomes clear from results that there exist optical activity that induces a rotation to the input linearly polarized source when laser light propagates through the bulk and the waveguide. The bulk response (black squares) arises from the intrinsic birefringence for *a*-cut crystal. While for the waveguides (red circles), as it can be seen from Fig. 6, there is a loss of polarization degree, so the end point of the electric field at the output does not describe the typical ellipse [27]. The output field becomes partially non-polarized after its propagation through the waveguide, suggesting that it is put forward an additional contribution of a kind of birefringence [1]. This effect can be associated to the coupling of the field corresponding to *quasi*-TM and *quasi*-TE modes, similar behavior was reported in Nd:YVO_4 by using ULI technique [28]. However, those waveguides have a larger cross section size and other writing geometry was used. By other side, it is reasonable to take the analysis of [29] as starting point to infer how the laser writing works in different materials. As it has already been reported [2,29], in *a*-cut $LiNbO_3$ and others but cubic crystalline (Nd:YAG, Nd:GGG) waveguides that only TE modes can be supported along inscribed double-track type II waveguides. $LiNbO_3$ as well as LiSAF have trigonal crystalline cell, nevertheless in latter TM propagation is admitted. Therefore the expansion direction, discussed in Ref. [29], which consider *elasto*-optic model [30] could give rise a deeper discussion about what properties determines the directions where the refractive index become incremented due to the laser writing interaction.

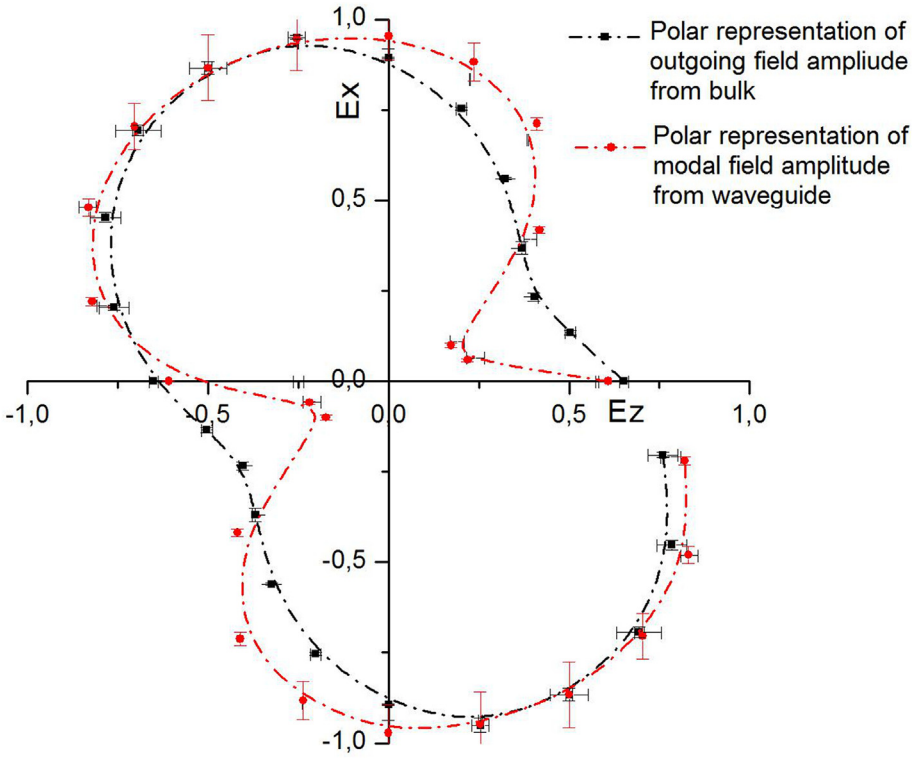

Fig. 6. Polar representation of both normalized output field amplitude of a double-track waveguide made with 3 μJ of energy per pulse and a writing speed of 30 μm/s and normalized field amplitude outgoing from bulk. Input was set linearly polarized at 45° respect to the work table.

It should be remarked that these measurements just show a qualitative comparison for quasi-TM and quasi-TE modes because the input angle and the TE and TM modes order should be taken into account to determine quantitative values. Finally a thorough study of polarization effects of this kind of waveguides structures should be carefully be made but it is out of scope of this work.

3.2. Spectroscopic measurements

In Fig. 7 we present the luminescence spectral mapping of a double-track waveguide written at 3 μJ. The different curves correspond to the different points explored inside the waveguide cross-section. The scheme of these points is illustrated in the inset figure, a micro-luminescence spectrum was taken for each point. Not all spectra records were included for sake of clarity. Also, the intensity was rescaled for each curve in order to avoid overlapping of the spectra. Considering the spectral resolution, the spectra do not present any variation of shape and the peak position comparing the different points of the waveguide cross-section scanned.

Following the spectroscopic analysis, in Fig. 8 the luminescence decay signals (in logarithmic scale) corresponding to $^4T_2 \rightarrow {}^4A_2$ transition for bulk (open black square) and waveguides (open red circles) are presented. This figure also includes fitting of the lifetime (solid line) corresponding to each case. For both lifetime decays, the fit provides 68μs considering the final uncertainty. The linear fitting was performed by R-square weighted adjust. Weights for terms of Chi-square correspond to the reciprocal square of the uncertainty bar sizes of each data point (error bars are showed in the figure). The uncertainty assigned to each data point increase gradually assigning the instrumental error at the beginning up to time corresponding to very low signal to noise ratio. On this zone (tail of the signal decay), the uncertainty is dominated by the standard deviation, the mean value was taken by average of the tail data points, and also was considered as the baseline to subtract it to all data points. The choice of the zero line is critical to test linear behavior provided that the plots were set in a logarithmic scale.

Therefore, if the changes of crystalline field that the Cr^{3+} ions undergo are small enough for the corresponding variation in the optical transition to be lower than the spectral resolution, it is possible to estimate an upper limit of induced stress. In this sense, we have conducted a rough estimation of this value by the following way. First we related the variation of 10Dq parameter with unitary deformation on the basis of microscopically dependence of the former with ligand distance between ions Cr^{3+} and nearest anions Al, called R, in an octahedral environment. This relationship was taken from Ref. [31], which also provides the dependence of the R with the lattice parameter. This, actually corresponds to Cr:LiCAF, but is expected to present a similar behavior for Cr:LiSAF. The relationship between 10Dq and unitary deformation ε can be written as:

$$\left(\frac{10Dq_o/B}{10Dq/B}\right)^{\beta/m} = \varepsilon + 1 \qquad (1)$$

where $10Dq_o$ is the value of crystalline field of our crystal while $10Dq = 10Dq_o + \Delta$, where Δ is the crystalline field variation induced by stress. B is the Racah parameter, while $\beta = 2$ and $m = 2.3$ according to [31]. Then, if 2 cm^{-1} is the experimental resolution in the luminescence spectrum, by using the slope of $^4T_2$ level in the TS diagram, Δ/B was calculated. Finally, by using the elasticity matrix [32], the coefficient stress σ_ζ, along c -direction where the maxima compression is expectable [28,30] could be estimated in 10 MPa as the upper limit. Calculation implies the knowledge of the position in the TS diagram ($10Dq_o$) as well as the Racah parameter B. The former was determined by an absorption

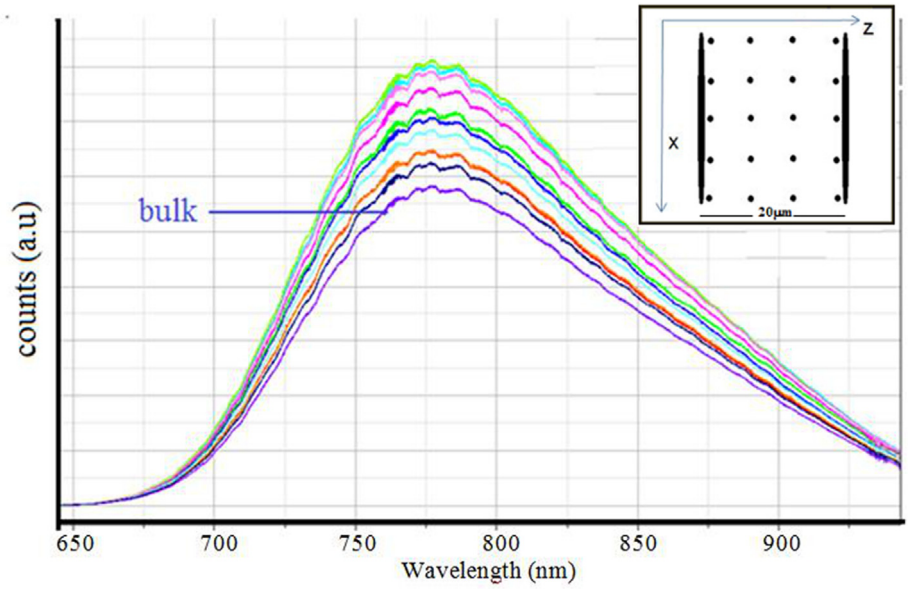

Fig. 7. Spectra of micro-luminescence experiments. The different colors curves correspond to different coordinate points inside the waveguide cross-sections which are illustrated in the inset as an array between laser tracks (dark ellipses oriented in the X direction (*a*-orientation)). The array of points indicates the sites in which each micro-luminescence spectrum was taken. The writing process was made moving the beam perpendicular to the XZ plane (*a*-*c* plane) at several velocities. It is possible to appreciate that there are no changes in the peak position or in the FWHM when comparing all spectra. Each spectrum scale was manipulated by an intensity factor only for visualization purposes. (For interpretation of the references to colour in this figure legend, the reader is referred to the web version of this article.)

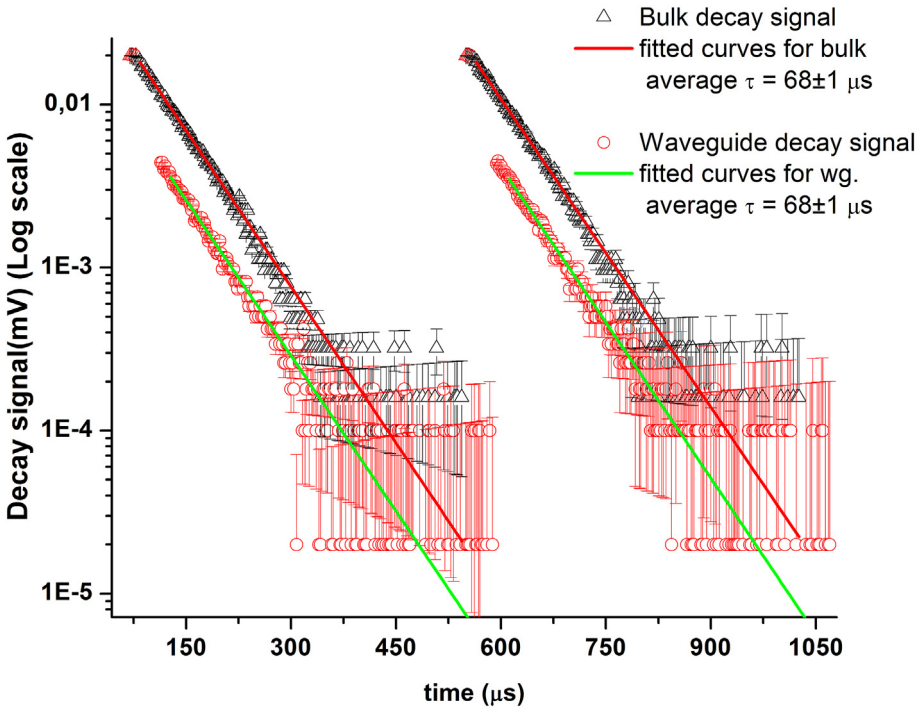

Fig. 8. This figure shows the experimental data collected by the oscilloscope after pumping the Cr^{3+} ions in bulk as well as in waveguides pumping the $^4T_2$ level with a pulsed laser diode centered at 650 nm of wavelength. The inset table states the average lifetimes (in μs units) obtained after fitting sequent decay signals.

spectrum corresponding to Cr^{3+} ions in the crystal considering the ratio between involved transitions energies while the latter was calculated from the absorption and emission spectra giving a value of $B = 725(5)\ cm^{-1}$.

4. Conclusions

For the first time, optical waveguides fabricated by femtosecond laser micromachining in Cr:LiSAF are reported. This crystal was shown to be suitable specie for laser writing applications. We explored a wide range of energies per pulse of fabrication and concluded that double-track guiding performance was acceptable for micromachining energies above 1 μJ, whose losses were lower than 2 dB/cm, for waveguides made up to 3 μJ per pulse. Considering single track waveguides, coupled light only was possible for those systems made at higher energies (>6 μJ).This suggests that

arise an important increment in the induced stress at the boundary of the focal volume zone which in turn, implies a higher contrast of induced refractive index.

Waveguides written at intermediate energies have shown single mode confinement and suitable propagation performance. In contrast, waveguides fabricated at higher energies, have presented a multimodal propagation performance at a wavelength of 632.8 nm, showing an enlarged guiding region with non-uniform modal shape due to the irregular borders.

It is also important to remark that all waveguides supported both quasi-TE and quasi-TM polarization guiding modes. For all polarization studies we also found optical activity after propagation in the waveguides which can be associated to the induced birefringence and/or to TM-TE mode coupling.

By inspection of the luminescence from the waveguides, could be showed that luminescent features were preserved with respect to the bulk for both, the emission spectrum and the lifetime. Measurements were performed in the structure fabricated with the highest energy per pulse, in which it was expected that the crystalline environment of the Cr^{3+} ions would be modified because of the level of induced stress. However, no peak shifting or FWHM modification was found, and therefore direct writing by femtosecond pulses is a potentially excellent method from a technological point of view. In this sense, by using the Tanabe Sugano representation, even roughly, we have estimated a value for the induced stress in the waveguide region by the laser writing process, being this equal to 10 MPa as an upper limit.

Acknowledgment

The authors would like to thank to Dr. Fabian Videla for the experimental support in lifetime measurements and fruitful discussions, and also to Dr. Dafne Amaya for helping us in image processing. This work was partially supported by the Agencia Nacional de Promoción Científica y Tecnológica under project PICT-2016-4086.

References

[1] R. Osellame, G. Cerullo, R. Ramponi (Eds.), “Femtosecond Laser Micromachining” Topics in Applied Physics, 2012.
[2] F. Chen, J.R.V. de Aldana, Optical waveguides in crystalline dielectric materials produced by femtosecond-laser micromachining, Online, Laser & Photonics Rev. 8 (2) (2013, May) 251–275, http://dx.doi.org/10.1002/lpor.201300025. Avaliable:.
[3] C.H. Hsieh, P.H. Tu, J.Y. Jeng, Area of modification within transparent materials by femtosecond laser, Adv. Mater. Res. 557–559 (2012) 1336–1339. Available at: http://dx.doi.org/10.4028/www.scientific.net/amr.557-559.1336.
[4] M.C. Richardson, et al., Ablation and Optical Property Modification of Transparent Materials with Femtosecond Lasers Presented at Laser-induced Damage in Optical Materials: 2003, 2004, http://dx.doi.org/10.1117/12.530684. Available at:.
[5] M. Fox, Properties of Solids, Oxford University Press, New York, 2001.
[6] E. Cantelar, D. Jaque, G. Lifante, “Waveguide lasers based on dielectric materials, Optical Materials 34 (3) (2012) 555–571, http://dx.doi.org/10.1016/j.optmat.2011.05.012. Available at:.
[7] W. Koechner, Properties of solid-state laser materials, in: Solid-state Laser Engineering, sixth ed., Springer Series in Optical Sciences, U.S.A, 2006.
[8] S.A. Payne, et al., Laser performance of LiSrAlF6:Cr^{3+}, J. Appl. Phys. 66 (3) (1989) 1051, http://dx.doi.org/10.1063/1.343491. Available at:.
[9] http://www.optoscience.com/maker/castech/lineup/Cr_LiSAF.html.
[10] S.A. Payne, L.K. Smith, R.J. Beach, B.H.T. Chai, J.H. Tassano, L.D. DeLoach, , et al.W.F. Krupke, Properties of Cr:LiSrAlF$_6$ crystals for laser operation, Appl. Opt. 33 (24) (1994) 5526, http://dx.doi.org/10.1364/ao.33.005526. Avaliable:.
[11] R.C. Powell, Transition-metal-ion laser materials [Internet]. Springer Nature, Phys. Solid-State Laser Mater. (1998) 254–293, http://dx.doi.org/10.1007/978-1-4612-0643-9_7. Available from:.
[12] M. Stalder, B.H.T. Chai, M. Bass, Flashlamp pumped Cr:LiSrAlF6 laser, Appl. Phys. Lett. 58 (3) (1991) 216, http://dx.doi.org/10.1063/1.104693. Available at: .
[13] Diode-pumped Mode-locked LiSAF Laser, Feb. 1996.
[14] R. Knappe, K.-J. Boller, R. Wallenstein, Single-mode continuous-wave Cr^{3+}: LiSAF ring laser pumped by an injection-locked 670-nm broad-area diode laser, Opt. Lett. 20 (19) (1995) 1988.
[15] U. Demirbas, et al., Femtosecond Cr:Colquiriite lasers pumped by a single tapered diode laser, in: T. Graf, et al. (Eds.), Laser Sources and Applications, 2012, http://dx.doi.org/10.1117/12.920539. Available at:.
[16] U. Demirbas, A. Sennaroglu, F.X. Kärtner, J.G. Fujimoto, Highly efficient, low-cost femtosecond Cr^{3+}:LiCAF laser pumped by single-mode diodes, Online, Opt. Lett. 33 (6) (2008) 590. Available: http://www.mirsurg.eu/mirs_5/Agnesi2.pdf.
[17] R.E. Samad, et al., Development of a flashlamp-pumped Cr:LiSAF laser operating at 30 Hz, Appl. Opt. 45 (14) (2006) 3356, http://dx.doi.org/10.1364/ao.45.003356. Available at:.
[18] J.-M. Hopkins, et al., Highly compact and efficient femtosecond Cr:LiSAF lasers, IEEE J. Quantum Electron. 38 (4) (2002) 360–368, http://dx.doi.org/10.1109/3.992549. Available at:.
[19] A. Rodenas, G.A. Torchia, G. Lifante, E. Cntelar, F. Jaque, D. Jaque, L. Roso, Refractive index change mechanisms in femtosecond laser written ceramic Nd:YAG waveguide lasers: micro-spectroscopy experiments and beam propagation calculations, Appl. Phys. B 95 (2009) 85–96.
[20] S. Sugano, Y. Tanabe, H. Kamimura, Multiplets in optical spectra, in: Multiplets of Transition Metal Ions in Crystals, Academic Press, New York 1970, 1970, pp. 106–125.
[21] B. Henderson, G.F. Inbush, Optical Spectroscopy of Inorganic Solids, Oxford Science Publications, Oxford, U.K., 1989.
[22] J.G. Solé, L.E. Bausá, D. Jaque, An Introduction to the Optical Spectroscopy of Inorganic Solids, 2005, Aug. 18, http://dx.doi.org/10.1002/0470016043 [Online]. Available at:.
[23] P.J. Chandler, X. Huang, P.D. Townsend, N. Hamelin, Y.T. Chow, Cr:LiSrAlF6 optical waveguides defined by ion beam implantation, Nucl. Instrum. Methods Phys. Res. Sect. B Beam Interact. Mater. Atoms 127–128 (1997) 528–532, http://dx.doi.org/10.1016/s0168-583x(96)00985-8. Available at:.
[24] A. Majkić, G. Poberaj, R. Degl'Innocenti, M. Döbeli, P. Günter, Cr:LiSrAlF6 channel waveguides as broadband fluorescence sources, Appl. Phys. B 88 (2) (2007) 205–209, http://dx.doi.org/10.1007/s00340-007-2708-5. Available at:.
[25] G. Lifante, Integrated Photonics: Fundamentals, Wiley-Blackwell, 2003, Jan., http://dx.doi.org/10.1002/0470861401. Available at:.
[26] R. Regener, W. Sohler, Loss in low-finesse Ti:LiNbO3 optical waveguide resonators, Appl. Phys. B 36 (3) (Mar. 1985) 143–147.
[27] M. Born, E. Wolf, Principles of Optics, Pergamon Press, U. K, 1980.
[28] F. Chen, J.R.V. de Aldana, Optical waveguides in crystalline dielectric materials produced by femtosecond-laser micromachining, Laser & Photonics Rev. 8 (2) (2014) 251–275, http://dx.doi.org/10.1002/lpor.201300025.
[29] M.R. Tejerina, D.A. Biasetti, G.A. Torchia, Polarization behaviour of femtosecond laser written waveguides in lithium niobate, Opt. Mater. 47 (2015) 34–38, http://dx.doi.org/10.1016/j.optmat.2015.06.030. Available at:.
[30] M.R. Tejerina, D. Jaque, G.A. Torchia, A “2D μ-Raman analysis of low repetition rate femto-waveguides in lithium niobate by using a finite element model, Opt. Mater. 36 (5) (2014) 936–940, http://dx.doi.org/10.1016/j.optmat.2013.12.040. Available at:.
[31] A. Trueba, J.M. García-Lastra, J.A. Aramburu, P. García-Fernández, M.T. Barriuso, M. Moreno, Pressure-induced changes in Cr^{3+}-doped elpasolites and $LiCaAlF_6$: interpretation of macroscopic data, Phys. Rev. B 81 (23) (Jun. 2010).
[32] Weber, J. Marvin (Eds.), Handbook of Optical Materials, CRC Press, 2003.